Brussels, Date 15th December 2014

Authors: Antonio Garcia-Uceda Juárez
Charles Hirsch

3rd International Workshop on Higher-Order CFD Methods

NUMECA Int., Chaussée de la Hulpe 189 Terhulpse Steenweg,
BE - 1170 Brussels, Belgium
Tel.: +32 (0)2 6478311, Fax.: +32 (0)2 6479398
www.numeca.com

1. Code description.

The results presented in this report have been obtained with a high-order Euler solver based on the novel Flux Reconstruction (FR) method (Huynh H.T. (2007)(2009)). This is implemented in the unstructured solver FINE/Open[tm], and handles every element topology (Hexas, Prisms, Tetras, and Pyrams) on hybrid meshes. In FR scheme the governing equations are solved in its differential form, thus no numerical integration is required as opposed to Discontinuous Galerkin (DG) methods.

The numerical solution $u(x)$ within each element is represented by a nodal basis that spans a polynomial space of order p. Solution values u_i that support this nodal basis are computed at defined locations within the reference element, being the degrees of freedom of the problem. These correspond to a 2D tensor product of Gauss points on Quad, and the so-called Williams-Shunn points in Williams D.M. (2013), on Trians. 3D elements Hexas and Prisms, respectively, are formed by tensor product with Gauss points in the 3rd dimension. A mapping $\mathbf{X}(\xi,\eta,\zeta)$ between the reference and real elements is constructed through isoparametric transformation. Curvilinear boundaries can be represented by Serendipity mapping, on both Hexas and Prisms, up to cubic order (see Zienkiewicz R.L. et al. (2005) for details).

In order to ensure consistency of the governing equations in differential form, a $C0$ continuous Flux function F(x) is constructed through the so-called correction functions (see Huynh H.T. (2007) for details), recovering a nodal-type DG scheme. These functions on Trians are computed following the approach in Huynh H.T. (2011). Resulting correction functions in 3D elements are the result of tensor product with the one “DG recovering” function in the 3rd direction. Explicit time integration is performed using a low-storage Runge-Kutta (RK) scheme of 4th order.

2. Case Summary.

The case presented is the C1.2: Flow over the NACA0012 airfoil, Inviscid Subsonic Flow. Subsonic characteristic inflow and outflow conditions are imposed at the farfield, corresponding to a Mach number of 0.5, and flow angle of 2º, as well as static atmospheric pressure. Finally slip wall conditions are imposed on the airfoil surface.

Simulations are performed on two sets of five nested structured meshes, composed of quads and trains, and orders p=1,2,3. The first set of meshes is of 140, 560, 2240, 8960, 35840 elements. The second set of meshes is of 280, 1120, 4480, 17920, 71680 elements. Second and third grids of each type are shown in figures 1-2. On the airfoil surface, elements are curved by quadratic Serendipity mapping, where the middle point on each boundary edge is mapped to the real geometry.

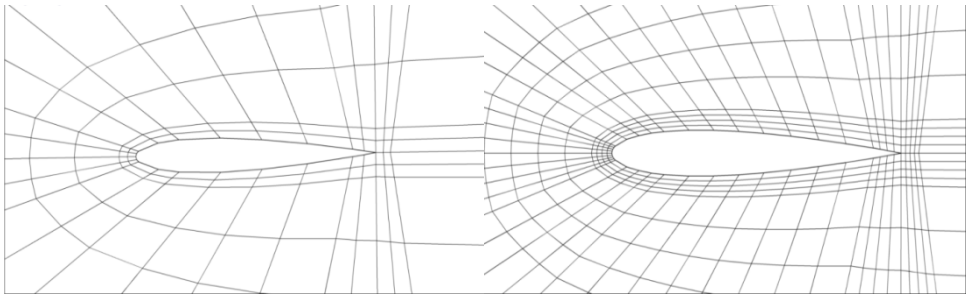

Figure 1: Meshes of 560 (left) and 2240 (right) quad elements.

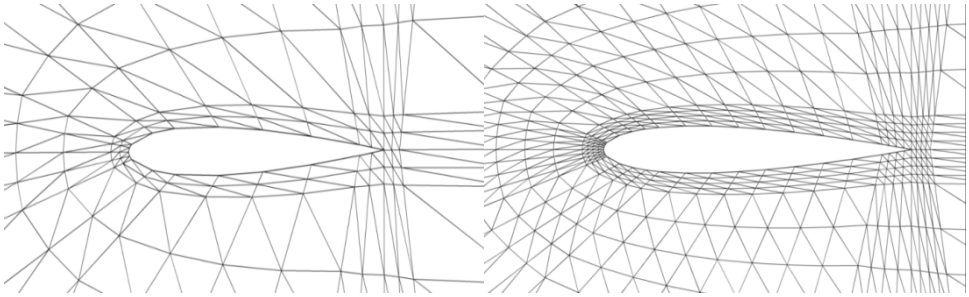

Figure 2: Meshes of 1120 (left) and 4480 (right) trian elements.

Simulations are started from an uniform flow of Mach number 0.5 and angle 2º Convergence is assumed when the L2 norm of the continuity equation residual drop below 10^{-7}. The accuracy of the scheme is assessed through the computation of the lift and drag coefficients as follows:

$$\vec{\boldsymbol{F}} = (F_x, F_y) = \sum^{nbFace} \int_{\Omega} (p - p_{ref}) \cdot \vec{n} dS$$

$$C_d = \frac{\cos(\theta) * F_x + \sin(\theta) * F_y}{0.5\rho_\infty {u_\infty}^2 s_{ref}}, \qquad C_l = \frac{-\sin(\theta) * F_x + \cos(\theta) * F_y}{0.5\rho_\infty {u_\infty}^2 s_{ref}}, \qquad \theta = 2º$$

Where integrals are calculated by a quadrature rule of sufficient order. The reference lift and drag are $Cd = 4.664340 \cdot 10^{-6}$ and $Cl = 2.864086 \cdot 10^{-1}$, provided by the RWTH Aachen University. It was not feasible to obtain reference data with the FR solver due to very large computation times.

3. Results.

Solutions obtained on the meshes of 560 and 2240 quads, and 1120 and 4480 trians, are displayed in figures 3-7 and 8-13, respectively. Simulation with p=3 on the 1120 trian mesh was not possible due to large geometrical distortion when attempting to curve the boundary cells, leading to negative Jacobian values within the boundary cells. Also results with p=2,3 on the finest trian meshes are not displayed in figure 12 due to incomplete convergence at the moment of this report.

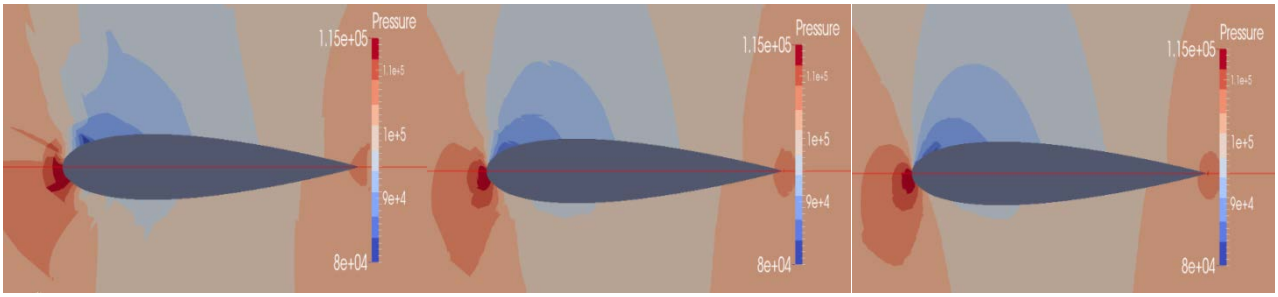

Figure 3: Contours of static pressure, on mesh of 560 quad elements. From left to right: p=1, 2, 3.

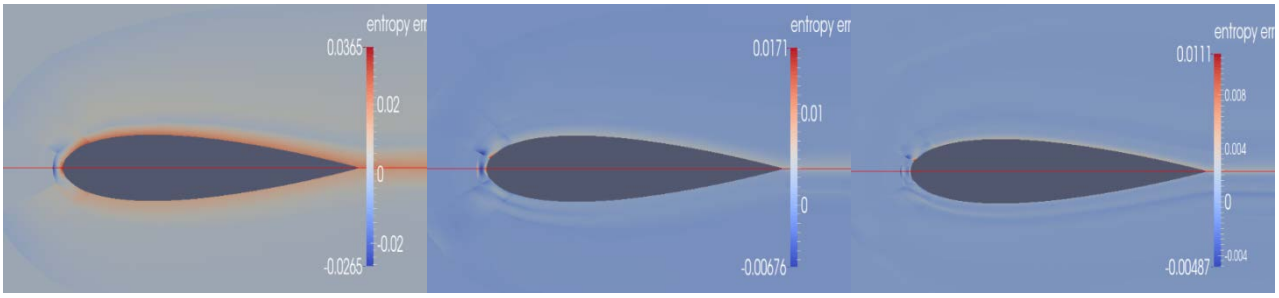

Figure 4: Contours of entropy error, on mesh of 560 quad elements. From left to right: p=1, 2, 3.

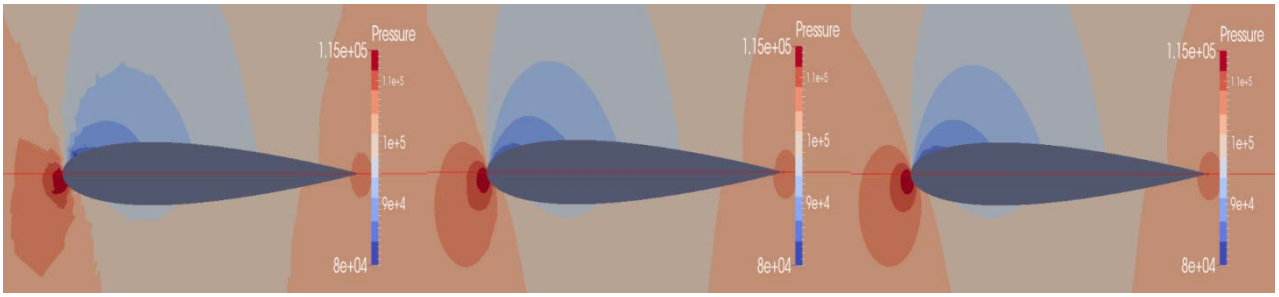

Figure 5: Contours of static pressure, on mesh of 2240 quad elements. From left to right: p=1, 2, 3.

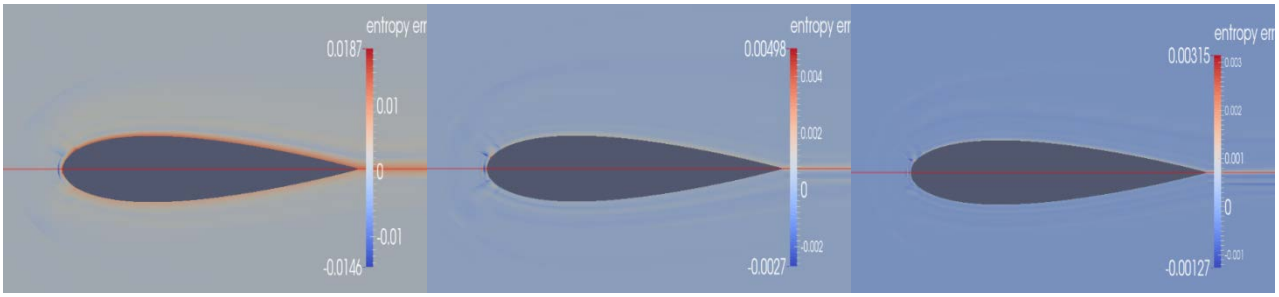

Figure 6: Contours of entropy error, on mesh of 2240 quad elements. From left to right: p=1, 2, 3.

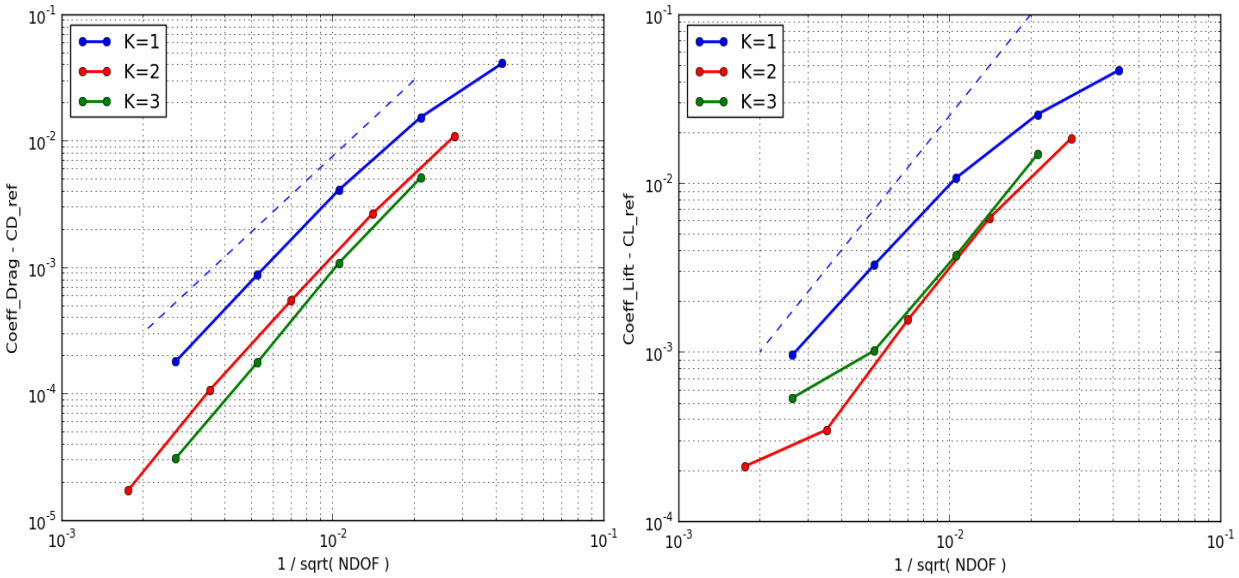

Figure 7: Error in Drag (left) and Lift (right) coefficients – characteristic length scale, on quad meshes. Theoretical slope is displayed in dashed line, only for p=1.

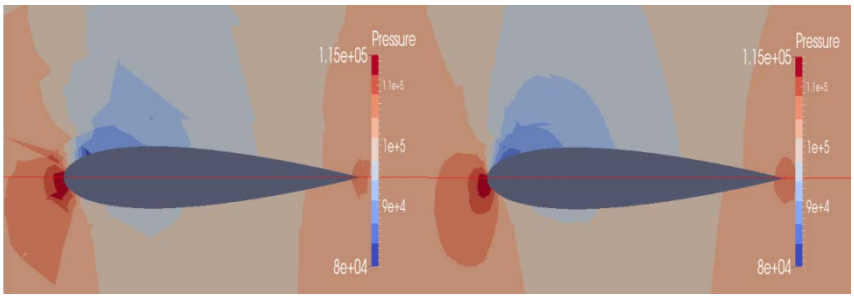

Figure 8: Contours of static pressure, on mesh of 1120 trian elements. From left to right: p=1, 2.

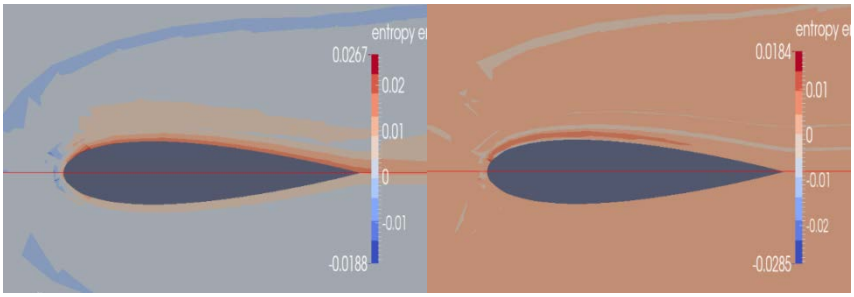

Figure 9: Contours of entropy error, on mesh of 1120 trian elements. From left to right: p=1, 2.

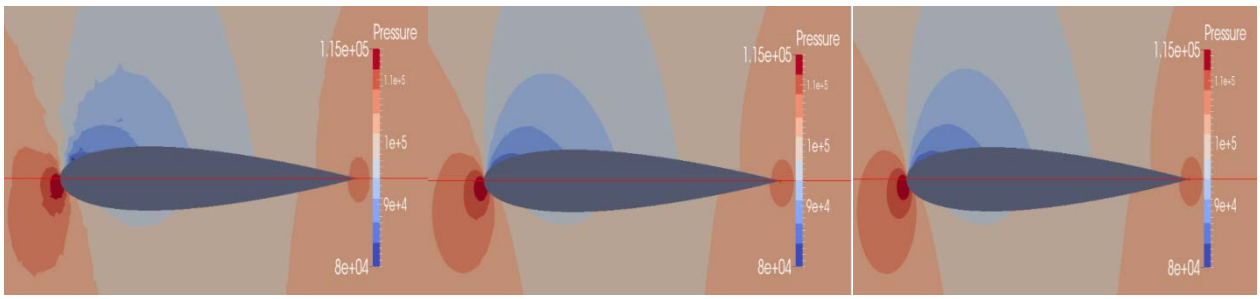

Figure 10: Contours of static pressure, on mesh of 4480 trian elements. From left to right: p=1, 2, 3.

n.v. NUMERICAL MECHANICS APPLICATIONS INTERNATIONAL s.a.
Office address : Chaussée de la Hulpe, 189, Terhulpesteenweg - 1170 Brussels - Belgium
www.numeca.com - Tél: +32 2 647 83 11 - Fax: +32 2 647 93 98 - BTW-TVA:BE 0447 480 893
Bank Accounts : BNP Paribas Fortis : 210-0420 099-44 - Dexia : 068-2406 673-33

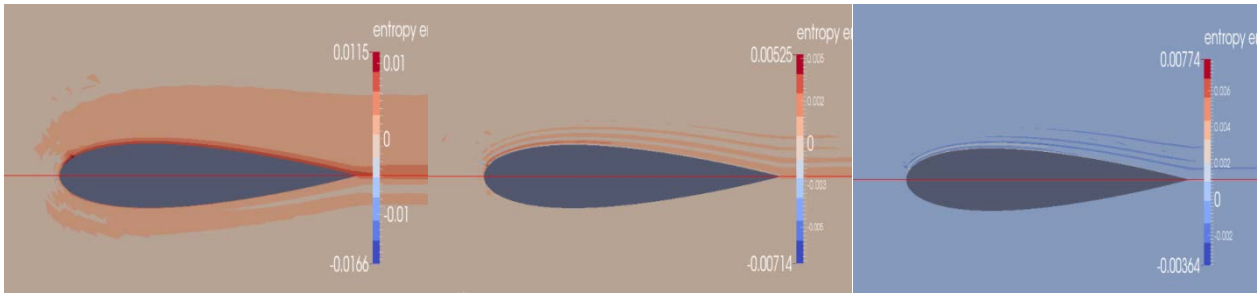

Figure 11: Contours of entropy error, on mesh of 4480 trian elements. From left to right: p=1, 2, 3.

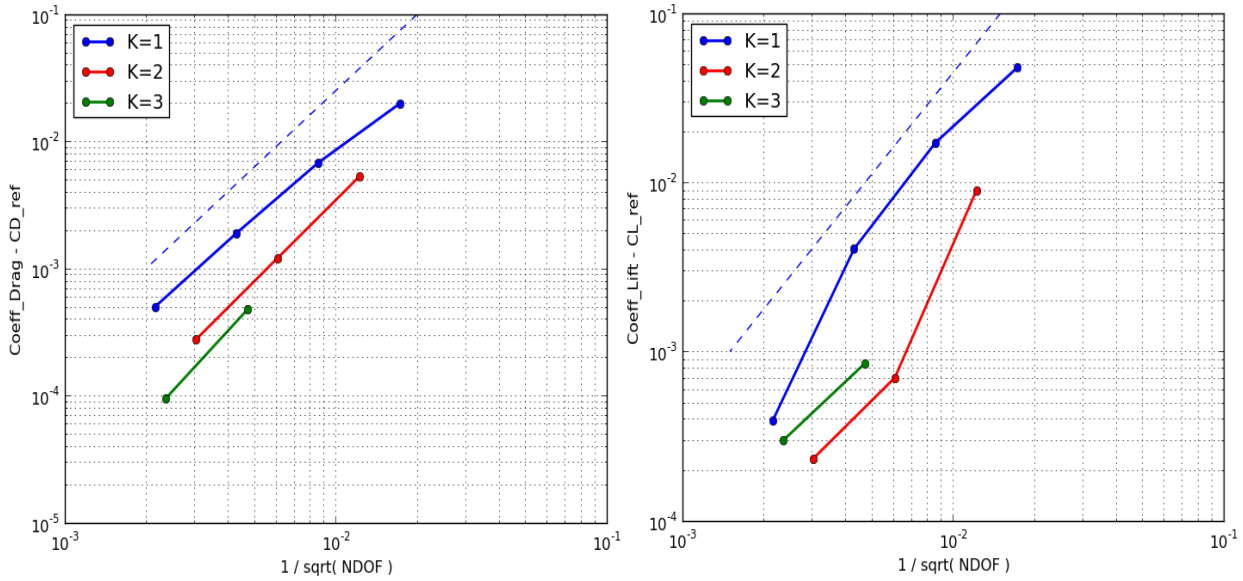

Figure 12: Error in Drag (left) and Lift (right) coefficients – characteristic length scale, on trian meshes. Theoretical slope is displayed in dashed line, only for p=1.

4. Conclusions.

Inviscid subsonic flow around NACA0012 airfoil has been performed successfully with the FR solver, on both quads and trian meshes. Converged solution has been achieved for all meshes and orders p, and it is clearly shown in figures 3-7 and 8-12 how solution accuracy is increased as either mesh-h or order-p is refined. Residuals convergence did not show a monotone trend, resulting in extremely large times of computation, reason why work units data are not displayed in this report. Also the convergence criteria needed to be relaxed to 10^{-7}.

On figures 7 and 12 it is shown how convergence rates on drag and lift coefficients, for schemes p=2,3, do not show the expected 3rd and 4th order accuracy respectively, but 2nd order (p=1) instead. The reason for this is being investigated. Perhaps the use of 2nd Serendipity mapping on curved boundaries is limiting the accuracy provided by the p=2,3 schemes, and higher-order representation is required. However, this option is not available at the moment of this report.

5. References.

Huynh H.T. (2007), A Flux Reconstruction Approach to High-Order Schemes Including Discontinuous Galerkin Methods. *AIAA Paper 2007-4079.*

Huynh H.T. (2009), A Reconstruction Approach to High-Order Schemes Including Discontinuous Galerkin for Diffusion. *AIAA Paper 2009-403.*

Huynh H.T. (2011), High-Order Methods Including Discontinuous Galerkin by Reconstuction on Triangular Meshes. *AIAA Paper 2011-44.*

Williams D.M. (2013), Energy-Stable High-Order Methods for Simulating Unsteady, Viscous, Compressible Flows on Unstructured Grids. *PhD thesiss, Stanford University*.

Zienkiewicz R.L., Taylor R.L., Zhu J.Z. (2005), The Finite Element Method: Its Basis and Fundamentals. *Elsevier, Butterworth Helneman.*